# Band theory of linear and nonlinear susceptibilities of some binary ionic insulators

W. Y. Ching, Fanqi Gan,* and Ming-Zhu Huang
*Department of Physics, University of Missouri–Kansas City, Kansas City, Missouri 64110*
(Received 8 September 1994; revised manuscript received 4 April 1995)

The linear and nonlinear optical responses in a large number of cubic insulators are studied by means of first-principles local-density calculations. Complete results on band structures, frequency-dependent dielectric functions, and frequency-dependent third-order nonlinear susceptibilities $\chi^{(3)}(\omega)$ (in the simplest form as the third-harmonic generations) are presented for 27 alkali halides, alkali-earth fluorides, oxides, and sulfides. They are LiF, LiCl, LiBr, LiI, NaF, NaCl, NaBr, NaI, KF, KCl, KBr, KI, RbF, RbCl, RbBr, RbI, $CaF_2$, $SrF_2$, $CdF_2$, $BaF_2$, MgO, CaO, SrO, BaO, MgS, CaS, and SrS. The results are compared with the existing experimental data and other calculations. The effectiveness of using a "scissor operator" to correct the gap underestimation in the local-density-approximation theory is assessed. It is shown that the full band-structure approach for the $\chi^{(3)}(0)$ calculation in these crystals gives results in very good agreement with experimental data, especially in the anisotropic coefficient of the nonvanishing tensor elements.

## I. INTRODUCTION

Recently, there have been increased activities in first-principles-type calculations on nonlinear optical properties of semiconductors and insulators using the band-theoretical approach.[1–10] In particular, second-harmonic generations (SHG's) and third-harmonic generations (THG's) of 18 semiconductors and their frequency-dependent dispersion relations were studied by Huang and Ching.[2,3] The band structures were calculated using the self-consistent orthogonalized linear combination of atomic orbitals (OLCAO) method (Ref. 11) in the local-density approximation (LDA). Nonlinear susceptibilities were evaluated with the application of a scissor operator to address the problem of gap underestimation that roots from the inadequacy of the LDA theory for the excited states, and the effect of the local field was totally neglected. The results of these calculations were in quite good agreement with the available experimental data. It was concluded that the accuracy of high conduction-band (CB) wave functions is extremely important because of the large CB-CB optical matrix elements involved in the nonlinear optical process. It was also pointed out that the sum over the band states must be carried out to include a sufficiently large number of CB states for a well-converged result.

Like the cubic semiconductors, binary ionic insulators also have interesting nonlinear optical properties. Because of the inversion symmetry in these crystals, there is no SHG, and the THG is the lowest order of optical nonlinearity. Many ionic insulators are important materials in electro-optical applications and in laser technology.[12] More recently, alkali-earth sulfides and halides doped with rare-earth elements have been considered as promising candidates for a generation of optical memory storage media.[13,14] Adair, Chase, and Payne measured nonlinear refractive indices (which relates to THG coefficients) on a large number of insulating crystals.[12] They compared the measured data with that predicted by the empirical formula of Boling, Glass, and Owyong.[15] The empirical formula relates the nonlinear refractive index $n_2$ to the linear refractive index $n_0$ for optical materials with low $n_0$. It has been a fairly common practice among researchers to estimate the nonlinear refractive indices of insulators using linear refractive data alone.[16–18]

Early theoretical work on alkali-halide crystals was based on the concept that the nonlinear polarizability of an ionic crystal can be obtained as the sum of anionic and cationic polarizabilities constructed by empirical means.[19,20] In a series of papers,[21–23] Lines used bond-orbital theory to study the linear and nonlinear optical responses in ionic crystals, and also the influence of the *d* orbitals in transition-metal oxides.[23] The intention was to develop a simple yet effective theory for linear and nonlinear optical responses in ionic crystals that goes beyond the rather crude independent ion model. Empirical formulas were derived to calculate the linear dielectric constants and nonlinear refractive indices of many ionic crystals with remarkable success if only the relative data were compared.[21,22] More sophisticated calculations of the hyperpolarizabilities (equivalent to the THG coefficient) in alkali halides had been attempted in a cluster-type calculation within the many-body perturbation scheme,[24] and also by using a time-dependent LDA theory.[25,26] These work appear to be the only first-principles type of calculations for the nonlinear response in ionic crystals. In the work of Johnson, Subbaswamy, and Senatore,[26] the calculation of hyperpolarizability had to rely on the use of pseudopotentials because of the numerical difficulty associated with the kinetic-energy correction. It is therefore logical and timely to apply the first-principles full band-structure approach to study the THG of simple ionic insulators with either rocksalt or fluorite structure in the same fashion as has already been demonstrated for the cubic semiconductors.

In this paper, we present results of calculations on the linear and nonlinear optical properties of LIF, LiCl,

0163-1829/95/52(3)/1596(16)/$06.00  

LiBr, LiI, NaF, NaCl, NaBr, NaI, KF, KCl, KBr, KI, RbF, RbCl, RbBr, RbI, $CaF_2$, $SrF_2$, $CdF_2$, $BaF_2$, MgO, CaO, SrO, BaO, MgS, CaS, and SrS. Our major focus is on the THG coefficients and the frequency-dependent dispersion relations for these 27 alkali halides, alkali-earth fluorides, oxides, and sulfides. Our approach of covering a large number of crystals for a comprehensive study is aimed at finding systematic trends in the properties of a whole class of materials, and in ascertaining the overall reliability of the band-theoretical method. The ability to calculate the frequency-dependent nonlinear optical spectrum is significant because most experimental measurements are carried out at finite frequencies. Also, nonlinear optical excitations near the band edge will be very different from that in the long-wavelength limit. The plan for this paper is as follows. In Sec. II, we briefly outline our method and procedures of calculation. Results for the band structures, and linear dielectric functions, are presented in Sec. III. Section IV deals with results of third-order nonlinear susceptibilities. In Sec. IV these results are further discussed in comparison with experimental data and other existing calculations.

## II. METHOD OF CALCULATION

Our method of calculation is strictly the same as for the cubic semiconductors.[1-3] The same band-theoretical method has also been used to study the electronic structure and linear optical properties of ten semiconducting wurtzite crystals.[27] Specifically, for each crystal, the self-consistent band structure using the experimental lattice constant is calculated first by means of the first-principles OLCAO method.[11] A full basis set consisting of atomic orbitals of the valence shell electrons plus the empty orbitals of the next shell is employed. Each orbital function is a product of a radial function in the form of linear combination of Gaussian-type orbitals (GTO's) and appropriate spherical harmonics. A full basis set is necessary for nonlinear optical calculation, since the accuracy of the high CB states is crucial.

The density of states (DOS) and the partial DOS are calculated based on the solutions of the LDA Kohn-Sham equations[28] at the 89 *ab initio* **k** points in the irreducible portion of the Brillouin zone (BZ). The linear optical properties are calculated based on the wave functions at the same 89 **k** points as were discussed before.[1] Past experience indicates that this level of **k**-point sampling is very adequate for the crystals under study.

The OLCAO method is noted for its efficiency and accuracy, as documented in many published articles.[11] In the present study, we made no specific attempt to optimize the calculation for either the electronic structure or the optical properties for each individual crystal. It is possible to improve the results slightly by optimizing the calculation by making a more judicious choice of basis or the fitting functions for each crystal. Nevertheless, our major goal in this paper is to investigate the third-order nonlinear susceptibility $\chi^{(3)}(\omega)$ for a whole class of insulators, and compare the results with experimental measurements[12] and those obtained by the empirical method.[22,23] We do not attempt to single out any particular crystal for a fully optimized treatment.

Because the LDA theory underestimates the band gap of insulators, it is imperative that we address this problem in optical studies. The density-functional theory,[28] and particularly its local approximation, is essentially a theory for the ground state of interacting electrons in solids and molecules.[29] A single exchange-correlation potential used in the Kohn-Sham equation is not adequate for insulators because of the discontinuity of the exchange-correlation potential across the gap region.[30-32] The real single-particle excitation gap differs from that of the LDA gap by a finite amount $\Delta$. Many papers have been written on these subjects, and different methods for gap correction have been deviced and tested with varying degrees of success.[33-43] However, the quasiparticle calculation in the *GW* approximation seems to indicate that the wave functions for the unoccupied CB, after the self-energy correction, differ very little from the LDA results.[34] This gives some justification to the use of the simple scissor operator scheme in performing complicated nonlinear optical calculations for insulators. The scissor operator amounts to a rigid shift of the CB states such that the experimentally reported gap is reproduced. In cubic semiconductors,[2,3] as well as in $\alpha$ quartz,[10] it has been shown that this simple scissor operator is quite effective in giving good results for nonlinear optical parameters. This is because the more elaborate many-body correction apparently makes very little change in the LDA wave functions as long as the momentum matrix elements (MME's) involved are evaluated accurately.

The nonlinear optical properties for the cubic ionic insulators are calculated using the band approach based on the analytic formulas presented by Moss, Ghahramani, and van Driel.[44] These authors have used the full band-structure approach and a minimal basis semi-*ab initio* method to calculate the THG of Si, Ge, and GaAs,[44] and also ZnSe, ZnTe, and CdTe.[45] We followed their approach in the calculation of SHG and THG for 18 semiconductors,[2,3] except that we employed self-consistent band structures with a full basis set and a much more rigorously calculated MME. In the calculation for the THG, we increase the number **k** points (with appropriate weighting factors) in the $\frac{1}{48}$ of the BZ to 505 for summation over the BZ. This amount of **k**-point sampling gives an accuracy of about 5% with respect to the **k**-space convergence $\chi^{(3)}$. One may be able to improve the **k**-space convergence by employing some kind of interpolation scheme, but we decided to use only the **k** points where the energy eigenvalues and the MME's are calculated *ab initio*.

The imaginary part of the complex $\chi^{(3)}(\omega)$ function consists of three contributions corresponding to the virtual-electron (VE), virtual-hole (VH), and three-state (3-*S*) processes.[44] The specific formulas for crystals with cubic symmetry suitable for computation were listed in Ref. 3. In the VE and VH processes, four states are involved. For the VE process, one state is in the valence band (VB) and three in the CB, and the MME products contain two CB-CB matrix elements. The VH process consists of three types (VH1, VH2, and VH3), one with

three states in the VB and one in the CB. The other two types have two states each in the VB and one in the CB. Only the last two types contain the CB-CB matrix in the MME product. In the 3-$S$ process, only three states are involved, one in the VB and two in the CB, and the MME product contains no CB-CB matrix element. This 3-$S$ contribution in $\chi^{(3)}(\omega)$ is different from the SHG calculation,[2] in which the MME product contains a CB-CB matrix element in a three-state transition. Since the CB-CB matrix elements are less accurate for highly excited states, the VE process, which contains the products of two CB-CB MME's will be less accurate compared with the other two processes. As was discussed before,[3] all three types of processes can make significant contributions and should not be neglected. The VE and VH processes make negative contributions, yet the overall sign of $\chi^{(3)}(0)$ is positive because the 3-$S$ term is dominating and positive.

We first evaluate the relevant VB-CB and CB-CB MME's, using the *ab initio* wave functions. The next step is to calculate the third-order susceptibility in the zero-frequency limit, $\chi^{(3)}(0)$, as a function of the CB energy cutoff using the simpler expressions

$$\chi^{(3)}(0)=\chi^{(3)}_{\rm VE}(0)+\chi^{(3)}_{\rm VH1}(0)+\chi^{(3)}_{\rm VH2}(0)+\chi^{(3)}_{\rm VH3}(0)+\chi^{(3)}_{3S}(0)\ , \tag{1}$$

where

$$\chi^{(3)}_{\rm VE}(0)=-\frac{2}{3}\left[\frac{e\hbar}{m}\right]^4\int_{\rm BZ}\frac{d\mathbf{k}}{4\pi^3}\sum_{ijkl}{\rm Re}[\mathbf{P}^{\rm vc}_{ij}\mathbf{P}^{\rm cc}_{jk}\mathbf{P}^{\rm cc}_{kl}\mathbf{P}^{\rm cv}_{li}][\mathcal{A}1+\mathcal{A}2+\mathcal{A}3]\ , \tag{2}$$

$$\chi^{(3)}_{\rm VH1}(0)=-\frac{2}{3}\left[\frac{e\hbar}{m}\right]^4\int_{\rm BZ}\frac{d\mathbf{k}}{4\pi^3}\sum_{ijkl}{\rm Re}[\mathbf{P}^{\rm vc}_{ij}\mathbf{P}^{\rm vv}_{li}\mathbf{P}^{\rm vv}_{kl}\mathbf{P}^{\rm cv}_{jk}][\mathcal{B}1+\mathcal{B}2+\mathcal{B}3]\ , \tag{3}$$

$$\chi^{(3)}_{\rm VH2}(0)=+\frac{2}{3}\left[\frac{e\hbar}{m}\right]^4\int_{\rm BZ}\frac{d\mathbf{k}}{4\pi^3}\sum_{ijkl}{\rm Re}[\mathbf{P}^{\rm vc}_{ij}\mathbf{P}^{\rm cc}_{jk}\mathbf{P}^{\rm vv}_{li}\mathbf{P}^{\rm cv}_{kl}][\mathcal{C}1+\mathcal{C}2+\mathcal{C}3]\ , \tag{4}$$

$$\chi^{(3)}_{\rm VH3}(0)=+\frac{2}{3}\left[\frac{e\hbar}{m}\right]^4\int_{\rm BZ}\frac{d\mathbf{k}}{4\pi^3}\sum_{ijkl}{\rm Re}[\mathbf{P}^{\rm vc}_{ij}\mathbf{P}^{\rm vv}_{li}\mathbf{P}^{\rm cc}_{jk}\mathbf{P}^{\rm cv}_{kl}][\mathcal{D}1+\mathcal{D}2+\mathcal{D}3]\ , \tag{5}$$

$$\chi^{(3)}_{3S}(0)=+\frac{2}{3}\left[\frac{e\hbar}{m}\right]^4\int_{\rm BZ}\frac{d\mathbf{k}}{4\pi^3}\sum_{ijkl}{\rm Re}[\mathbf{P}^{\rm vc}_{ij}\mathbf{P}^{\rm cv}_{jk}\mathbf{P}^{\rm vc}_{kl}\mathbf{P}^{\rm cv}_{li}][\mathcal{E}1+\mathcal{E}2]\ , \tag{6}$$

and

$$\mathcal{A}1=\frac{729}{(3E_{ki}-2E_{ji})(3E_{li}-E_{ji})E^5_{ji}}\ ,$$

$$\mathcal{A}2=\frac{128(2E_{ji}-E_{ki})}{(2E_{li}-E_{ki})(2E_{ji}-3E_{ki})(2E_{ji}+E_{ki})E^5_{ki}}\ ,$$

$$\mathcal{A}3=\frac{1}{(E_{ki}-2E_{li})}\left[\frac{1}{(E_{ji}-3E_{li})}+\frac{2E_{ki}}{(E_{li}+E_{ji})(E_{ki}+2E_{li})}\right]\frac{1}{E^5_{li}}\ ;$$

$$\mathcal{B}1=\frac{729}{(3E_{jl}-2E_{ji})(3E_{jk}-E_{ji})E^5_{ji}}\ ,$$

$$\mathcal{B}2=\frac{128(2E_{ji}-E_{jl})}{(2E_{jk}-E_{jl})(2E_{ji}-3E_{jl})(2E_{ji}+E_{jl})E^5_{jl}}\ ,$$

$$\mathcal{B}3=\frac{1}{(E_{jl}-2E_{jk})}\left[\frac{1}{(E_{ji}-3E_{jk})}+\frac{2E_{jl}}{(E_{jk}+E_{ji})(E_{jl}+2E_{jk})}\right]\frac{1}{E^5_{jk}}\ ;$$

$$\mathcal{C}1=\frac{729}{(3E_{ki}-2E_{ji})(3E_{kl}-E_{ji})E^5_{ji}}\ ,$$

$$\mathcal{C}2=\frac{128(2E_{ji}-E_{ki})}{(2E_{kl}-E_{ki})(2E_{ji}-3E_{ki})(2E_{ji}+E_{ki})E^5_{ki}}\ ,$$

$$\mathcal{C}3=\frac{1}{(E_{ki}-2E_{kl})}\left[\frac{1}{(E_{ji}-3E_{kl})}+\frac{2E_{ki}}{(E_{kl}+E_{ji})(E_{ki}+2E_{kl})}\right]\frac{1}{E^5_{kl}}\ ;$$

$$\mathcal{D}1=\frac{729}{(3E_{jl}-2E_{ji})(3E_{kl}-E_{ji})E^5_{ji}}\ ,$$

$$\mathcal{D}2=\frac{128(2E_{ji}-E_{jl})}{(2E_{kl}-E_{jl})(2E_{ji}-3E_{jl})(2E_{ji}+E_{jl})E^5_{jl}}\ ,$$

$$\mathcal{D}3=\frac{1}{(E_{jl}-2E_{kl})}\left[\frac{1}{(E_{ji}-3E_{kl})}+\frac{2E_{jl}}{(E_{kl}+E_{ji})(E_{jl}+2E_{kl})}\right]\frac{1}{E^5_{kl}}\ ;$$

$$\mathcal{E}1=\frac{729}{(3E_{jk}-E_{ji})(3E_{li}-E_{ji})E^5_{ji}}\ ,$$

$$\mathcal{E}2=\frac{1}{(E_{jk}+3E_{li})}\left[\frac{(E_{lk}+E_{jk})}{(E_{lk}-3E_{li})(E_{ji}+E_{li})}+\frac{(E_{ji}+E_{jk})}{(E_{ji}-3E_{li})(E_{lk}+E_{li})}\right]\frac{1}{E^5_{li}}\ .$$

In the above expressions, $i$, $j$, $k$, and $l$ are band indexes, $v$ and $c$ stands for VB or CB states, and $E_{ij}=E_i-E_j$. $\mathbf{P}_{ij}=-i\hbar\langle i|\nabla|j\rangle$ is the MME connecting states $i$ and $j$. Thus the element $\chi^{(3)}_{1111}(\omega)$ corresponds to the case where the bracket [ ] contains the product of four $x$ components of $\mathbf{P}$ in expressions (2)–(5) above.

It was pointed out by us[2,3] that a determination of the cutoff energy is necessary in order to ensure that the

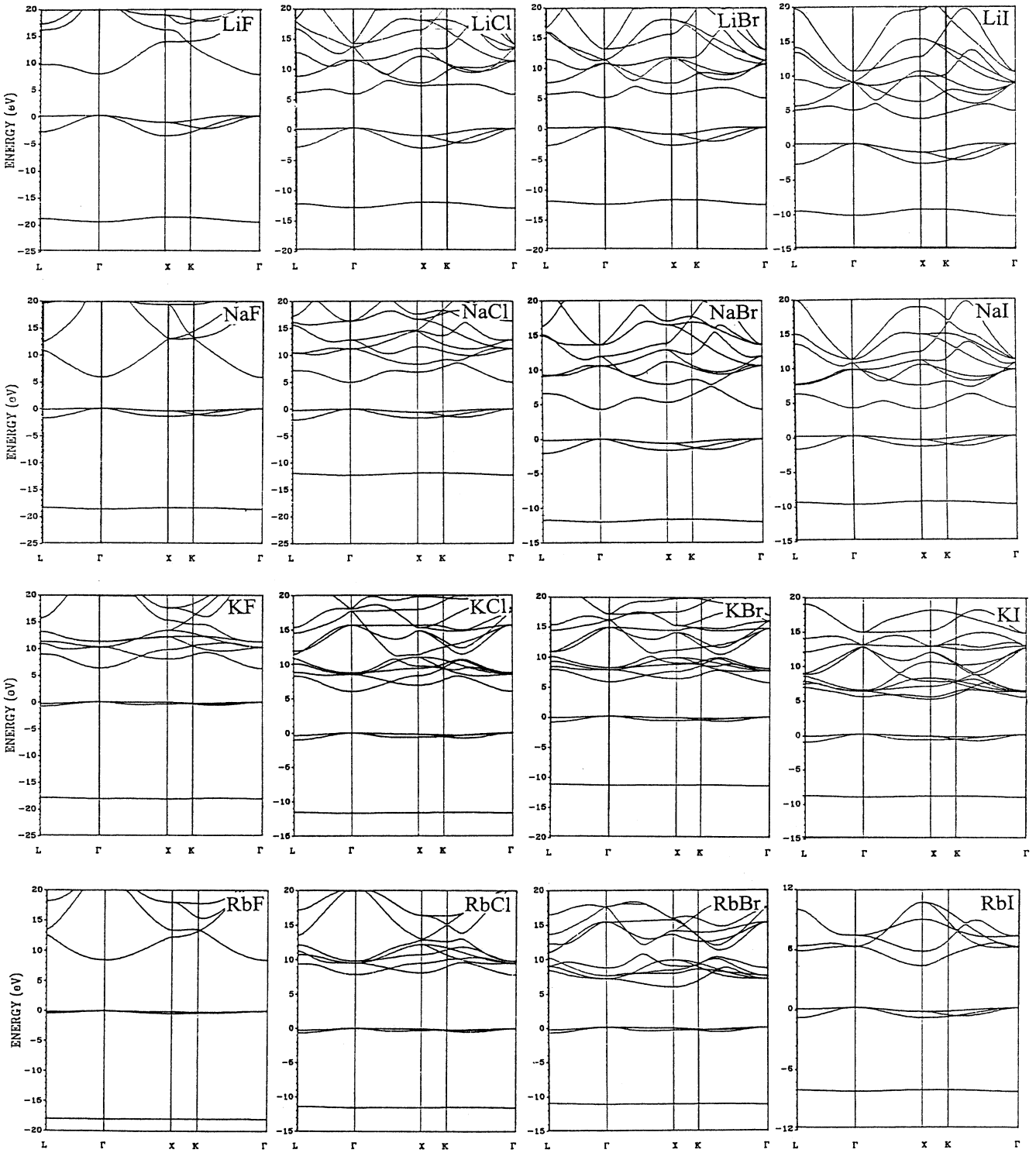


FIG. 1. Calculated band structures of alkali-halide crystals as indicated.

number of CB's used in the nonlinear optical calculation is sufficient. This cutoff energy is then used for the calculation of the dispersion relations. The imaginary part of $\chi^{(3)}(\omega)$, or $\mathrm{Im}[\chi^{(3)}(\omega)]$ is evaluated first, and the real part, or $\mathrm{Re}[\chi^{(3)}(\omega)]$, is obtained by Kramers-Kronig conversion. Finally, the absolute dispersion $|\chi^{(3)}(\omega)|$ is obtained from the real and imaginary components. It is clear from Eqs. (1), (2), and (3) listed in Ref. 3 that each type of contribution consists of a $\omega$ term, a $2\omega$ term, and a $3\omega$ term. It is the $3\omega$ term that is directly linked to the THG and is expected to dominate in the low-frequency region. The resonant $\delta$ functions in Eqs. (1)–(3) of Ref. 3 are evaluated using an energy window of 0.01 eV which is determined by detailed tests in order to be consistent with the number of **k** points used in the BZ sum. In crystals with cubic symmetry, there are two tensor elements of interest, the diagonal element $\chi^{(3)}_{1111}(\omega)$ and the off-diagonal element $\chi^{(3)}_{1212}(\omega)$, where the subscripts 1, 2, and 3 stand for Cartesian directions. We have evaluated both elements for frequencies up to 12 eV. The ratio $\chi^{(3)}_{1212}(0)/\chi^{(3)}_{1111}(0)$ should be a more reliable indicator of the accuracy of the calculation, since systematic errors in the experimental measurements may be canceled out. For a completely isotropic medium, this ratio should be 1/3.

## III. RESULTS ON THE BAND STRUCTURES AND LINEAR OPTICAL PROPERTIES

There have been numerous past calculations for the band structures[46–60] of the crystals discussed in this paper using different methods, and, to a much lesser extent,

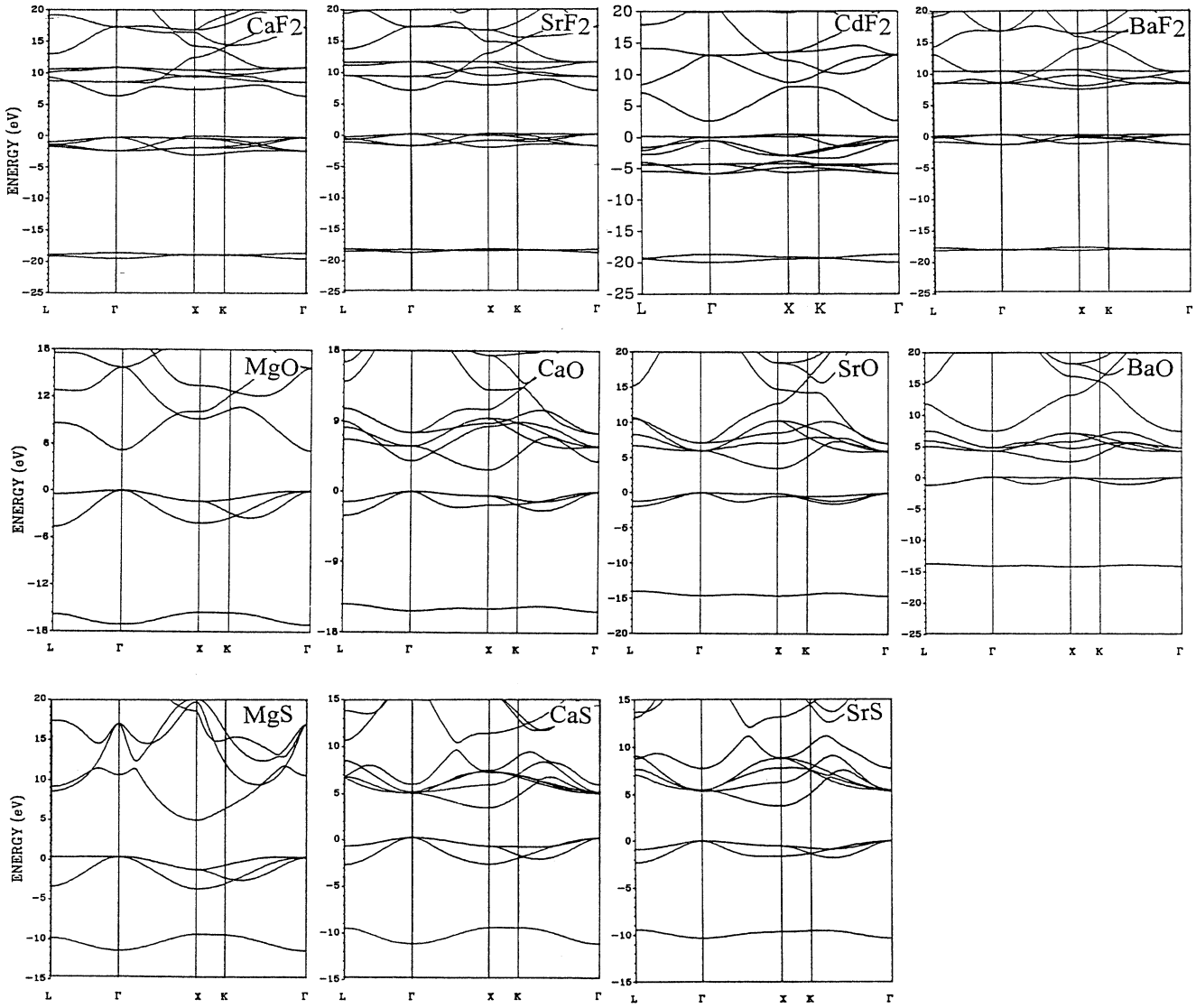


FIG. 2. Calculated band structures of alkali-earth fluorides, oxides, and sulfides as indicated.

the optical properties. We only cite some of the more recent ones. Recently, more advanced calculations[61] for the ground-state lattice dynamics and dielectric constants of alkali-earth oxides have been performed using the density-functional perturbation theory in conjunction with soft norm-conserving pseudopotential-plane-wave method. None of these studies were as comprehensive and systematic as the present study. *Ab initio* calculation of interionic potentials and cohesive properties of ionic crystals using different quantum-chemical methods have been reviewed by Pyper.[62] We will not review those past results or make any comparisons with our calculation, since our major focus is to present results for THG in these crystals obtained by using the first-principles band approach. However, a systematic study of the electronic structures and linear optical properties of all these crystals, calculated by a state-of-the-art method, is itself of considerable value and usefulness. We will therefore present our calculated results for the electronic structure and linear optical properties mostly in the form of tables and diagrams. We shall then concentrate our discussions on the nonlinear optical properties.

We divide the 27 crystals studied into seven groups in order to identify systematic trends within each group. They are (a) the Li halides (LiF, LiCl, LiBr, and LiI); (b) the Na halides (NaF, NaCl, NaBr, and NaI); (c) the potassium halides (KR, KCl, KBr, and KI); (d) the rubidium halides (RbF, RbCl, RbBr, and RbI); (e) the alkali-earth fluorides ($CaF_2$, $SrF_2$, $CdF_2$, and $BaF_2$); (f) the alkali-earth oxides (MgO, CaO, SrO, BaO); and (g) the alkali-earth sulfides (MgS, CaS, and SrS). Figures 1 and 2 show the calculated band structures of these seven groups

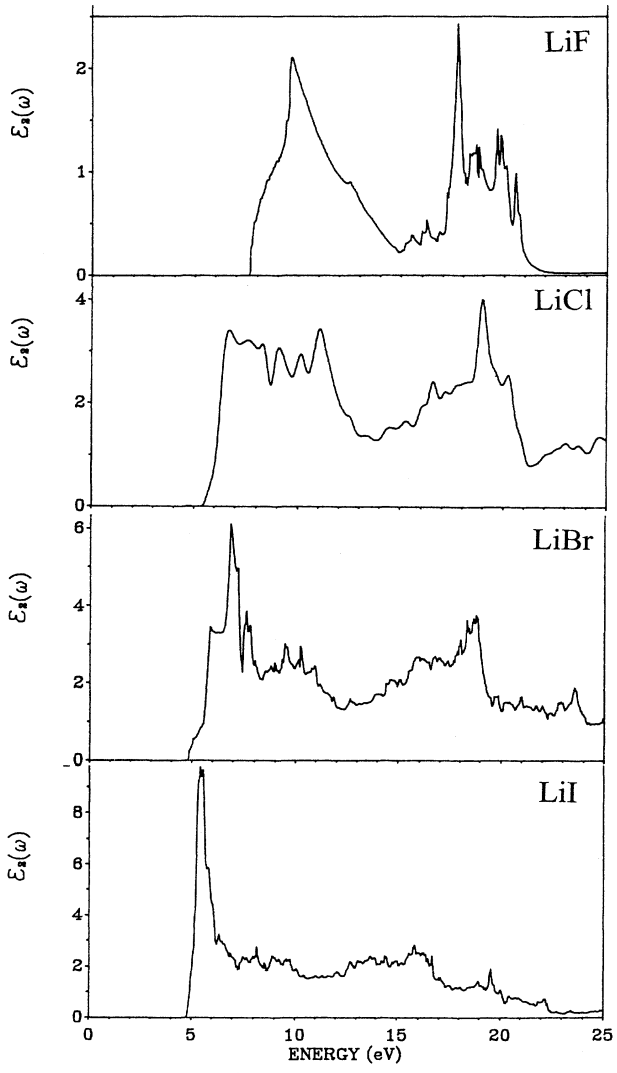


FIG. 3. Calculated $\varepsilon_2(\omega)$ of LiF, LiCl, LiBr, and LiI.

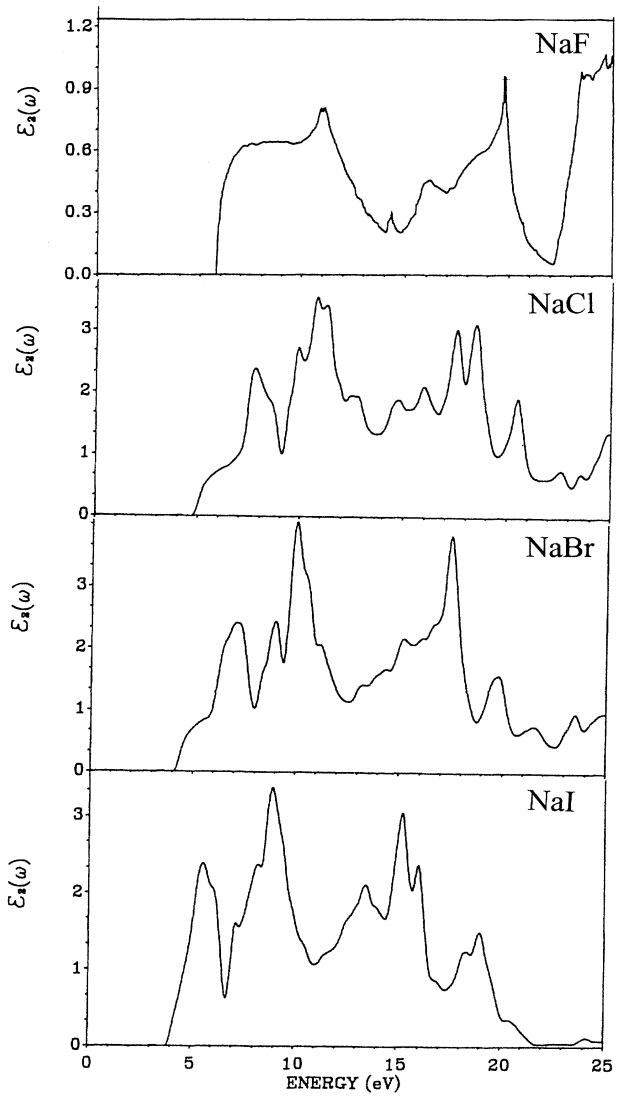


FIG. 4. Calculated $\varepsilon_2(\omega)$ of NaF, NaCl, NaBr, and NaI.

of insulators. The DOS's for each group are also calculated but are not presented here. (They can be obtained from the Physics Auxiliary Publication Service.) To make a better use of space, the energy scales in the band diagrams for each crystal are not fixed to be the same. In general, the band structures and the DOS within each group show a consistent trend. The difference is mostly reflected in the CB only. Since the high CB's have been shown to be important for nonlinear optical excitations, we expect the calculated THG for crystals within each group not to be very close. Other noticeable trends observed are as follows. (1) The upper VB width deceases from group (a) to group (d). (2) Most of the alkali halides have direct band gaps at $\Gamma$ except for the iodides, and also RbBr, where the bottom of the CB is at $X$ instead of $\Gamma$. The first three fluorides have the top of the VB at $X$, which are also very close in energy to that of $\Gamma$, and the bottom of the CB at $\Gamma$. However, for $BaF_2$, the bottom of the CB is at $X$ and the top of the VB is almost dispersionless. All the oxides and sulfides have indirect gaps with the bottom of the CB at $X$ except MgO, which has a direct gap at $\Gamma$. (3) Within the same group, the gap decreases as the atomic number $Z$ of the anion increases. (4) $CdF_2$ in group (e) is a marked exception because of the involvement of the semi-core-like Cd $3d$ states near the $-5$ to $-6.5$ eV region, and also in the lower CB region. This results in a relatively smaller gap for $CdF_2$ as compared to others in the series, which are all wide-gap insulators. (5) Comparing the results between the oxide group (f) and the sulfide group (g), we see their electronic

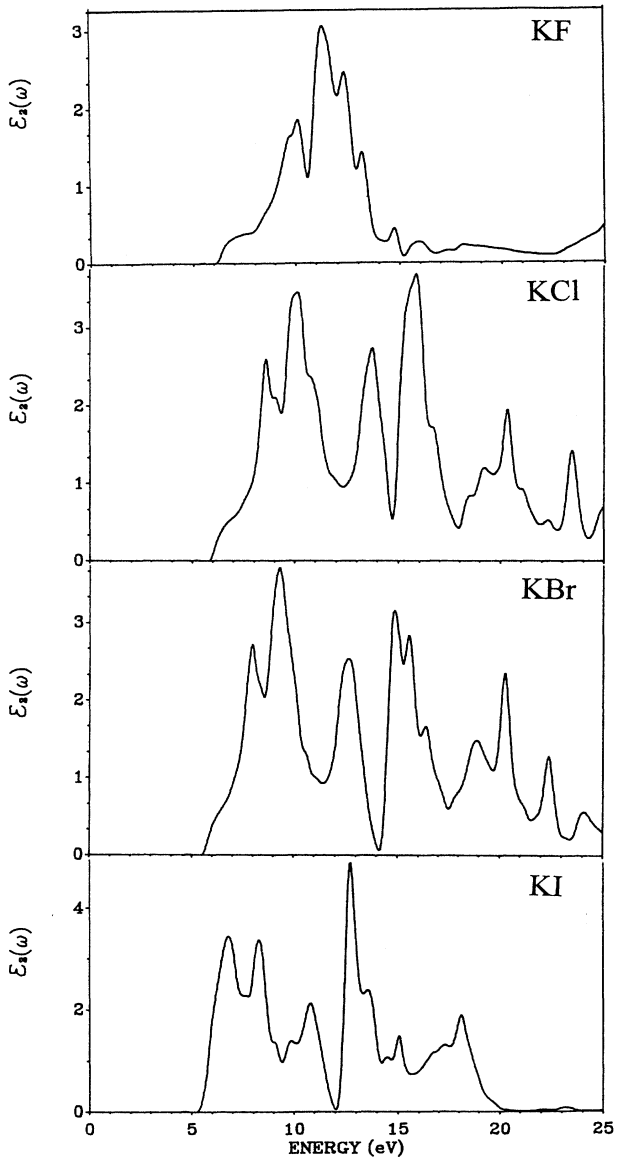


FIG. 5. Calculated $\varepsilon_2(\omega)$ of KF, KCl, KBr, and KI.

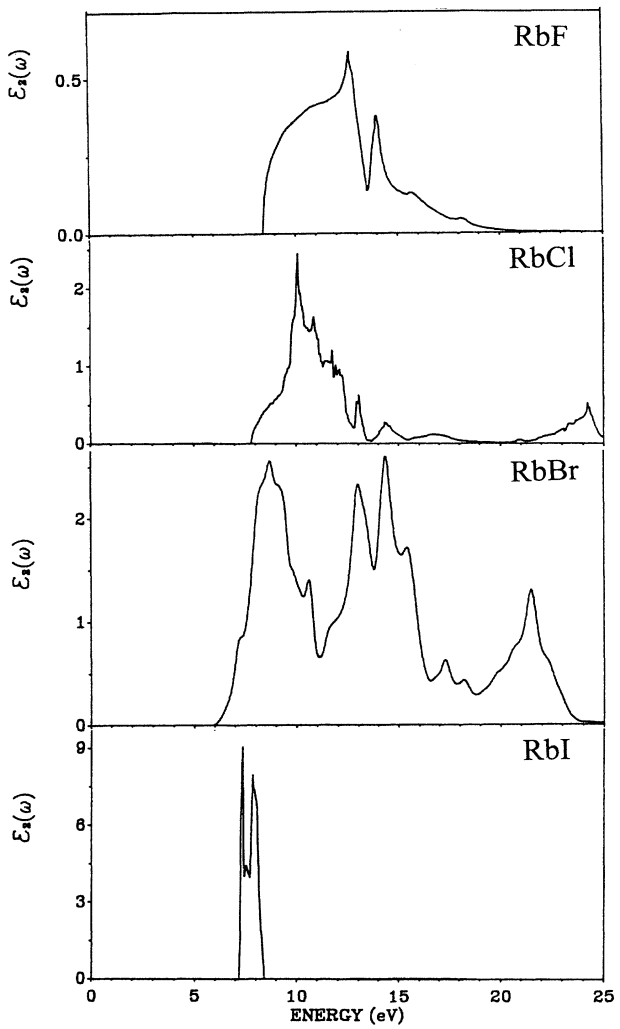


FIG. 6. Calculated $\varepsilon_2(\omega)$ of RbF, RbCl, RbBr, and RbI.

structures to be quite similar, as would be expected for the isoelectronic series. However, we note that the upper VB's for the sulfides are wider than that of oxides.

The calculated imaginary parts of the dielectric functions of the 27 insulators for photon energies up to 25 eV are shown in Figs. 3–9. As can be seen, the linear optical-absorption spectra vary greatly from crystal to crystal, even for those within the same series. This is because the CB's are usually quite different, and the symmetries of the wave functions which dictate the selection rules are fully reflected in the MME's. Optical calculations using the constant matrix approximation are generally unable to reflect such differences for crystals within the same series. The real parts of the dielectric functions $\varepsilon_1(\omega)$ were also obtained by Kramers-Kronig conversion but are not shown. In Table I, we list the lattice constants used in the calculation, the calculated LDA band gaps, and $\varepsilon_1(0)$, the zero-frequency limits interpreted as the static electronic dielectric constants. Also listed are the scissor operator shifts $\Delta$ used for each crystal, in order for the gap values to be close to the measured ones. For crystals where the experimental gap values are not well known, estimated values are used. For each crystal, two calculated $\varepsilon_1(0)$ values are listed: one obtained with gap correction using the scissor operator and the other with no correction. Also listed are the experimental

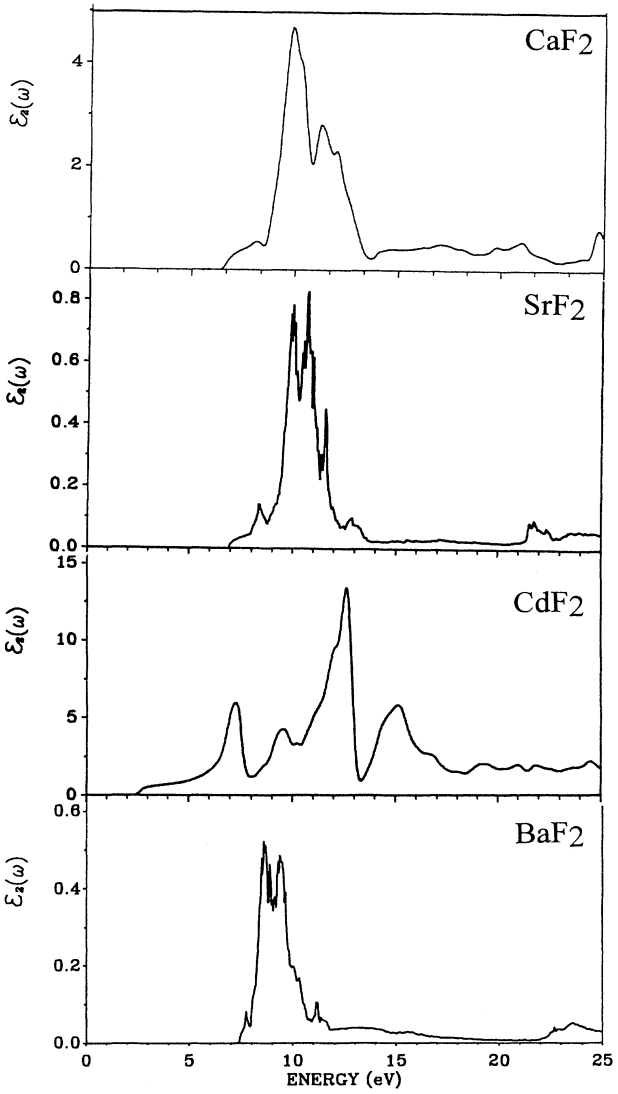


FIG. 7. Calculated $\varepsilon_2(\omega)$ of $CaF_2$, $SrF_2$, $CdF_2$, and $BaF_2$.

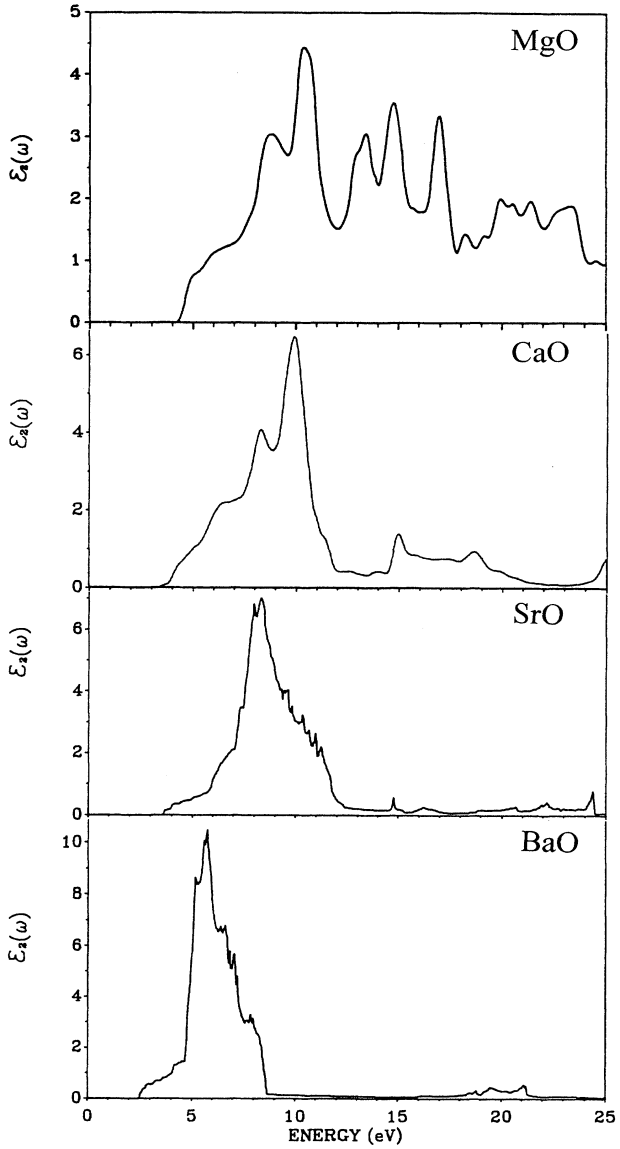


FIG. 8. Calculated $\varepsilon_2(\omega)$ of MgO, CaO, SrO, and BaO.

values for $\varepsilon_1(0)$ as listed in Ref. 21. We find that the general agreement for $\varepsilon_1(0)$ with the measured data is marginal. The scissor operator improves the agreement on some crystals, but not for Rb compounds and most of the alkali-earth compounds. It is not clear whether this has to do with the LDA theory or the fact that the experimental values may contain some lattice contributions to $\varepsilon_1(0)$. In most theoretical work, $\varepsilon_1(0)$ is usually treated as an input parameter determined by experiment. It has been pointed out by us in a number of publications that although the LDA theory underestimates the band gap in insulators,[27,58,59,63–68] the optical transition calculation without the gap correction can actually give better agreement in the peak positions than those with gap correction.[27,58,63–68] In this paper, we will not make any detailed analysis of the linear optical spectra or compare them with existing measurements or other calculations. It is our hope that our detailed calculations for these crystals can be a valuable source of information for future references and comparisons.

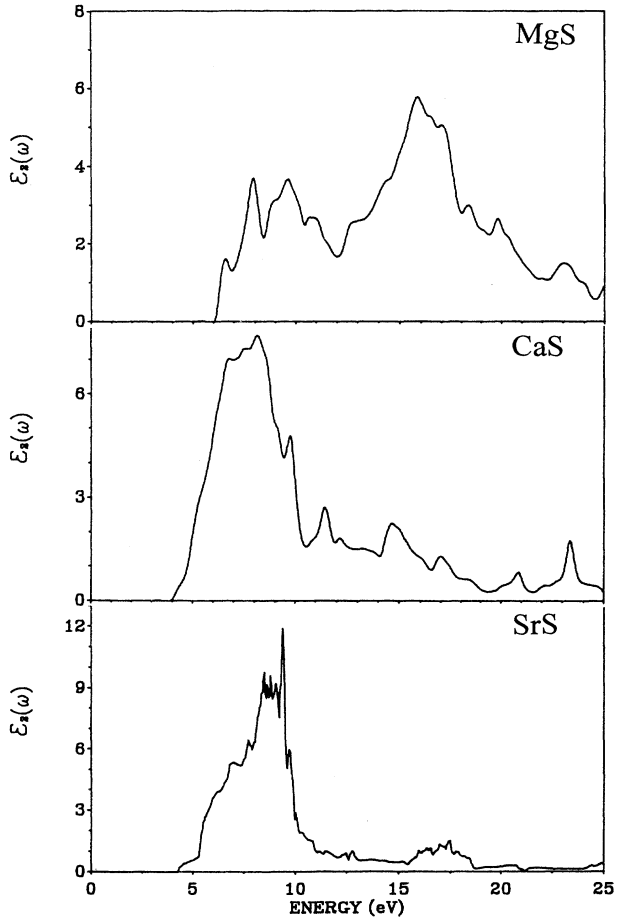


FIG. 9. Calculated $\varepsilon_2(\omega)$ of MgS, CaS, and SrS.

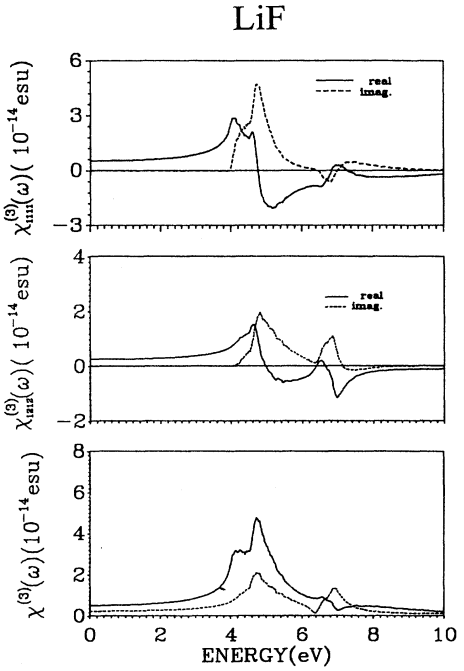


FIG. 10. Calculated THG for LiF: (a) $\chi^{(3)}_{1111}(\omega)$ and (b) $\chi^{(3)}_{1212}(\omega)$; the solid line is for the real part, and the dashed line for the imaginary part. (c) Solid line for $|\chi^{(3)}_{1111}(\omega)|$ and dashed line for $|\chi^{(3)}_{1212}(\omega)|$.

## IV. RESULTS ON NONLINEAR OPTICAL PROPERTIES

In this section, we present results of calculations of THG for the 27 cubic insulators. Like those for the cubic

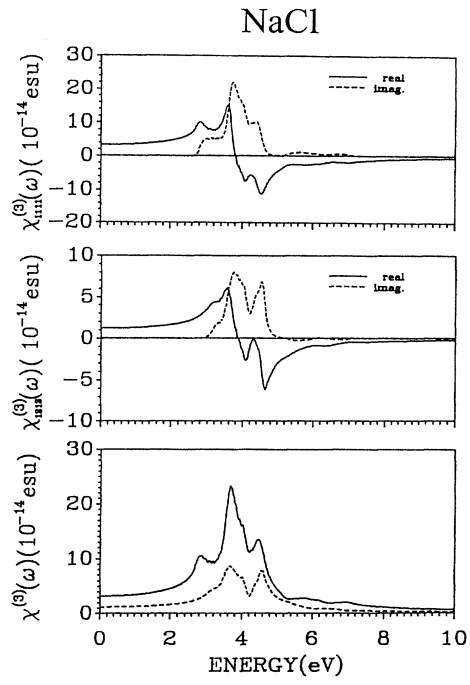


FIG. 11. Calculated THG for NaCl. Notations are the same as in Fig. 10.

semiconductors,[3] each calculation starts with the zero-frequency limits $\chi^{(3)}_{1111}(0)$ and $\chi^{(3)}_{1212}(0)$, which also test the CB cutoff energy that is needed for sufficient convergence. The cutoff energy for the THG calculation is usually less than that needed for the SHG calculation because the energy denominator in the THG goes as $E^7$, whereas that of the SHG goes as $E^5$, where $E$ is the energy denominator in the expressions for the nonlinear coefficients.[2,3] The unrestricted high-energy cutoff can lead to erroneous results because the wave functions obtained from a variational method may not be sufficiently accurate for high CB states, resulting in a large error in the CB-CB MME. All calculated $\chi^{(3)}(0)$ values for the insulators are positive, since it is dominated by the $3S$ process which makes a positive contribution to $\chi^{(3)}(0)$.[3] The CB cutoff energies and the calculated values for $\chi^{(3)}_{1111}(0)$ and $\chi^{(3)}_{1212}(0)$ obtained with gap corrections are listed in Table II. These values vary over two orders of magnitudes, ranging from $0.011\times10^{-13}$ esu in RbF to $6.23\times10^{-13}$ esu in SrS for $\chi^{(3)}_{1111}(0)$. Also listed for comparison are the calculated values by Lines using the bond-orbital method,[22,23] the time-dependent LDA result of Johnson, Subbaswamy, and Senatore,[26] and the empirical results using the formula of Boling, Glass, and Owyoung as presented by Adair, Chase, and Payne based on their measured data.[12] The measurements are actually for the nonlinear refractive index $n_2$, which is related to $\chi^{(3)}(0)$ by $\chi^{(3)}(0)=n_0n_2/3\pi$, where $n_0$ is the measured linear refractive index. It should be noted that this conversion expression differs from Eq. (2) of Ref. 12 by a factor of 4, which has to do with the proper definition for the $\chi^{(3)}(0)$ coefficient. In this paper, we follow the same definition for $\chi^{(3)}(0)$ as in our study for the semiconductors,[2,3] and convert all data to the same definition. The measured values are most likely obtained at the wavelength of 1 $\mu$m, or equivalently at the photon energy of 1.24 eV. The extrapolated values to zero frequency are expected to be slightly smaller. However, at the present level of accuracy in both the calculation and measurement, we will ignore this small difference. In principle, we can obtain the $|\chi^{(3)}(\omega)|$ values at a specific frequency from the calculated dispersion relations. Most likely, the

TABLE I. Calculated gap and static dielectric constant for cubic insulators.

| Crystal | $a$ (Å) | $E_g$ (eV) | $\Delta$ (eV) | $\varepsilon(0)$ (Calc.) no $\Delta$ corr. | $\varepsilon(0)$ (Calc.) with $\Delta$ corr. | $\varepsilon(0)$ (expt.) |
|---|---|---|---|---|---|---|
| LiF | 4.017 | 7.65($d$) | 4.6 | 4.09 | 3.60 | 1.92 |
| LiCl | 5.129 | 5.59($d$) | 3.9 | 3.50 | 2.17 | 2.68 |
| LiBr | 5.507 | 4.94($d$) | 2.7 | 5.64 | 3.03 | 3.00 |
| LiI | 6.000 | 3.55($id$) | 2.5 | 3.61 | 2.30 | 3.40 |
| NaF | 4.620 | 5.77($d$) | 4.5 | 2.66 | 1.74 | 1.74 |
| NaCl | 5.630 | 4.92($d$) | 3.5 | 3.48 | 1.88 | 2.33 |
| NaBr | 5.937 | 4.24($d$) | 3.2 | 3.05 | 1.91 | 2.60 |
| NaI | 6.473 | 3.80($id$) | 2.3 | 2.76 | 2.49 | 2.98 |
| KF | 5.347 | 6.26($d$) | 4.3 | 2.15 | 1.39 | 1.84 |
| KCl | 6.290 | 5.98($d$) | 2.3 | 2.87 | 2.43 | 2.17 |
| KBr | 6.600 | 5.76($d$) | 1.7 | 2.62 | 2.17 | 2.35 |
| KI | 7.066 | 5.07($id$) | 0.8 | 2.81 | 2.18 | 2.63 |
| RbF | 5.640 | 8.40($d$) | 1.6 | 1.14 | 1.10 | 1.93 |
| RbCl | 6.581 | 7.80($d$) | 0.2 | 1.43 | 1.38 | 2.17 |
| RbBr | 6.854 | 5.88($id$) | 1.0 | 2.00 | 1.77 | 2.34 |
| RbI | 7.342 | 4.16($id$) | 2.2 | 1.50 | 1.37 | 2.59 |
| $CaF_2$ | 5.460 | 6.53($d$) | 4.2 | 2.02 | 1.49 | 2.04 |
| $SrF_2$ | 5.800 | 6.77($id$) | 3.5 | 1.23 | 1.12 | 2.06 |
| $CdF_2$ | 5.388 | 2.01($id$) | 3.3 | 8.00 | 6.90 | 3.14 |
| $BaF_2$ | 6.200 | 7.19($id$) | 1.8 | 1.12 | 1.07 | 2.15 |
| MgO | 4.210 | 5.13($d$) | 3.2 | 4.28 | 3.10 | 2.95 |
| CaO | 4.810 | 2.91($id$) | 3.4 | 3.22 | 1.66 | 3.27 |
| SrO | 5.160 | 3.44($id$) | 2.5 | 3.04 | 1.90 | 3.35 |
| BaO | 5.520 | 2.44($id$) | 3.0 | 4.01 | 2.90 | 3.68 |
| MgS | 5.203 | 4.59($id$) | 1.8 | 5.12 | 4.52 | 4.84 |
| CaS | 5.690 | 3.20($id$) | 2.0 | 4.47 | 3.01 | 4.24 |
| SrS | 6.020 | 3.70($id$) | 1.2 | 3.68 | 2.78 | 4.09 |

photon frequency of interest is within the gap energy, where the imaginary part of $\chi^{(3)}(\omega)$ makes no contribution. However, the real part of $\chi^{(3)}(\omega)$ is obtained from the imaginary part by Kramers-Kronig conversion. This conversion process tends to reduce accuracy because the imaginary part can only be calculated up to a finite photon frequency. The calculated and measured anisotropic ratios of $\chi^{(3)}_{1212}(0)$ to $\chi^{(3)}_{1111}(0)$ are listed in Table III along with the experimental values.[12] Additional older data on the anisotropy are also listed for some of the crystals.[69,70] These ratios are better indicators for comparison purposes, since systematic errors in both $\chi^{(3)}_{1111}(0)$ and $\chi^{(3)}_{1212}(0)$ are expected to cancel out. We will discuss these results and their comparisons in Sec. V.

We have calculated the frequency-dependent THG dispersion relations for all 27 cubic insulators. Due to space limitations, we can only present the representative result, one from each group. Figures 10–16 show the real parts, imaginary parts, and absolute values of $\chi^{(3)}_{1111}(\omega)$ and $\chi^{(3)}_{1212}(\omega)$ for LiF, NaCl, KI, RbI, $CdF_2$, MgO, and CaS, respectively. The results for the other 20 crystals can be obtained from the Physics Auxiliary Publication Service. The main feature of interest is the structures in the dispersion relations. For most crystals, the THG dispersion relations have relatively simple features, consisting of a few peaks. For a few crystals (RbCl, $CaF_2$, $SrF_2$, $CdF_2$, CaS, and SrS), resonance structures exist at regions of higher photon energies. The validity and the significance of these higher-energy resonances cannot be established at this time. It is also noted that for most crystals, $|\chi^{(3)}_{1111}(\omega)|$ is always larger than $|\chi^{(3)}_{1212}(\omega)|$ except for KI, RbI, $SrF_2$, $CaF_2$, $BaF_2$, and MgS, where they are approximately equal. In general, low-frequency structures in $|\chi^{(3)}_{1111}(\omega)|$ and $|\chi^{(3)}_{1212}(\omega)|$ tend to be at the same positions. There are exceptions, however. In NaF, RbF, and BaO, the dominating peak in $|\chi^{(3)}_{1212}(\omega)|$ shifts to higher photon energy relative to the same peak in $|\chi^{(3)}_{1111}(\omega)|$. There are also cases (LiF, NaCl, NaBr, KI, $CaF_2$ $SrF_2$, and $CdF_2$) where there exist prominent structures in the low-energy side of $|\chi^{(3)}_{1111}(\omega)|$ that are totally

TABLE II. Calculated third-order susceptibilities $A=|\chi^{(3)}_{1111}(0)|$ and $B=|\chi^{(3)}_{1212}(0)|$ (in units of $10^{-13}$ esu). Experimental values (Ref. 12) are in parentheses. $A_L$, $A_{JSS}$, and $A_{BGO}$ are calculated values from Refs. 22, 26, and 12, respectively, converted to $|\chi^{(3)}_{1111}(0)|$. $E_c$ is the cutoff energy used in the calculation.

| Crystal | $E_c$ (eV) | $A$ (expt.) | | $A_L$ | $A_{JSS}$ | $A_{BGO}$ | $B$ (expt.) | |
|---|---|---|---|---|---|---|---|---|
| Lif | 20 | 0.052 | (0.038) | 0.173 | 0.071 | 0.059 | 0.024 | (0.017) |
| LiCl | 30 | 0.53 | | 1.08 | 0.35 | | 0.37 | |
| LiBr | 30 | 1.69 | | 1.93 | 0.62 | | 0.64 | |
| LiI | 30 | 2.84 | | 3.74 | 1.22 | | 1.77 | |
| NaF | 30 | 0.041 | (0.048) | 0.13 | 0.083 | 0.053 | 0.027 | (0.021) |
| NaCl | 35 | 0.32 | (0.26) | 1.19 | 0.33 | 0.37 | 0.20 | (0.097) |
| NaBr | 35 | 0.68 | (0.56) | 2.14 | 0.57 | 0.82 | 0.317 | (0.237) |
| NaI | 25 | 1.36 | | 4.58 | 1.08 | | 0.37 | |
| KF | 25 | 0.095 | (0.108) | 0.37 | 0.095 | 0.052 | 0.018 | (0.032) |
| KCl | 30 | 0.21 | (0.32) | 1.36 | 0.27 | 0.29 | 0.07 | (0.097) |
| KBr | 25 | 0.59 | (0.48) | 2.23 | 0.42 | 0.56 | 0.156 | (0.216) |
| KI | 25 | 4.68 | | 4.42 | 0.77 | | 2.92 | |
| RbF | 25 | 0.011 | | 0.47 | 0.13 | | 0.003 | |
| RbCl | 25 | 0.27 | | 1.53 | 0.31 | | 0.077 | |
| RbBr | 25 | 1.35 | | 2.34 | 0.48 | | 0.79 | |
| RbI | 25 | 2.10 | | 4.46 | 0.81 | | 1.59 | |
| $CaF_2$ | 25 | 0.075 | (0.065) | 0.25 | | 0.074 | 0.039 | (0.036) |
| $SrF_2$ | 30 | 0.070 | (0.076) | 0.334 | | 0.076 | 0.042 | (0.045) |
| $CdF_2$ | 30 | 0.55 | (0.65) | | | 0.23 | 0.17 | (0.21) |
| $BaF_2$ | 30 | 0.14 | (0.104) | 0.479 | | 0.11 | 0.077 | (0.068) |
| MgO | 30 | 0.40 | (0.294) | 0.69 | | | 0.21 | (0.142) |
| CaO | 30 | 0.63 | (1.00) | 1.44 | | | 0.27 | (0.262) |
| SrO | 30 | 1.04 | (0.99) | 2.49 | | | 0.55 | |
| BaO | 30 | 1.10 | | 4.58 | | | 0.52 | |
| MgS | 25 | 2.17 | | 4.134 | | | 1.43 | |
| CaS | 25 | 4.82 | | 5.487 | | | 2.80 | |
| SrS | 25 | 6.23 | | 6.376 | | | 3.80 | |

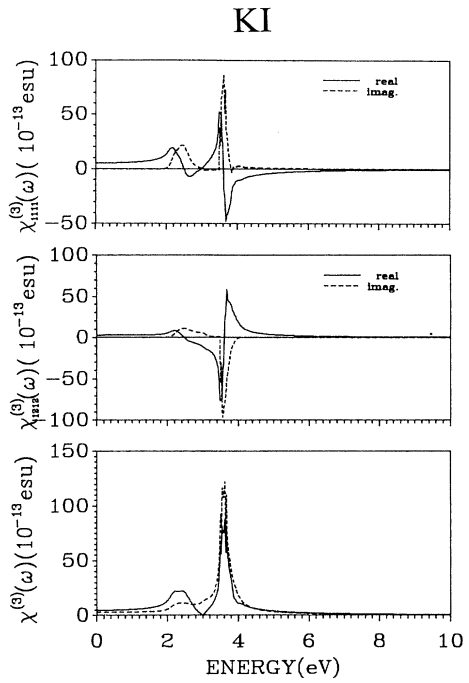


FIG. 12. Calculated THG for KI. Notations are the same as in Fig. 10.

absent in $|\chi^{(3)}_{1212}(\omega)|$. These minor variations in the spectral features of the THG reflect subtle differences in the electronic structures of different crystals. There are also large variations among different crystals in the amplitudes of $|\chi^{(3)}_{1111}(\omega)|$ and $|\chi^{(3)}_{1212}(\omega)|$, ranging from a low value of $0.12\times10^{-13}$ esu in KR to a high value of $170\times10^{-13}$ esu in RbI. However, within each series, the amplitude increases as the $Z$ value of the anion increases. This is clearly related to the size of the direct band gap at $\Gamma$. One marked exception is $CdF_2$, which has a rather small LDA gap of 2.01 eV at $\Gamma$, but a relatively modest value of $9.6\times10^{-13}$ esu for the maximum amplitude in $|\chi^{(3)}_{1212}(\omega)|$.

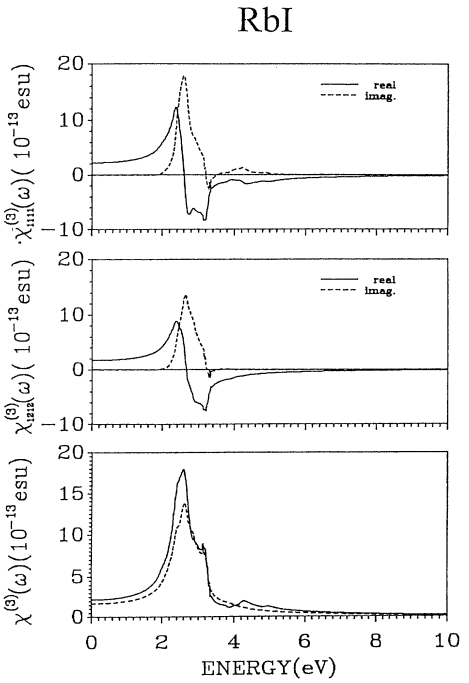


FIG. 13. Calculated THG for RbI. Notations are the same as in Fig. 10.

## V. DISCUSSION

The results for the THG in a large number of insulating crystals presented in Sec. IV enable us to make a better assessment of the current understanding of the nonlinear optical properties of ionic insulators. Previously, self-consistent first-principles calculations were limited only to alkali halides in the spherical shell approximation for the charge density in the static limit.[26] There are several advantages in using the first-principles band-structure approach to study the ionic solids. First, the

TABLE III. Calculated anisotropic ratio $|\chi^{(3)}_{1212}(0)|/|\chi^{(3)}_{1111}(0)|$. Experimental values are in parentheses.

| | |
|---|---|
| LiF | 0.46 (0.46,[a] 0.45[b]) |
| LiCl | 0.79 |
| LiBr | 0.38 |
| LiI | 0.62 |
| NaF | 0.66 (0.45[a]) |
| NaCl | 0.38 (0.37,[a] 0.43[b]) |
| NaBr | 0.47 (0.42[a]) |
| NaI | 0.27 |
| KF | 0.19 (0.29[a]) |
| KCl | 0.33 (0.30,[a] 0.30[b]) |
| KBr | 0.26 (0.45,[a] 0.37[b]) |
| KI | 0.62 |
| RbF | 0.27 |
| RbCl | 0.29 |
| RbBr | 0.59 |
| RbI | 0.76 |
| $CaF_2$ | 0.52 (0.56,[a] 0.50,[b] 0.44[c]) |
| $SrF_2$ | 0.60 (0.60,[a] 0.68[c]) |
| $CdF_2$ | 0.31 (0.32,[a] 0.32[b]) |
| $BaF_2$ | 0.55 (0.66,[a] 0.66[c]) |
| MgO | 0.53 (0.48,[a] 0.55[b]) |
| CaO | 0.43 (0.26[a]) |
| SrO | 0.53 |
| BaO | 0.47 |
| MgS | 0.66 |
| CaS | 0.58 |
| SrS | 0.61 |

[a]Reference 12.
[b]Reference 69.
[c]Reference 70.

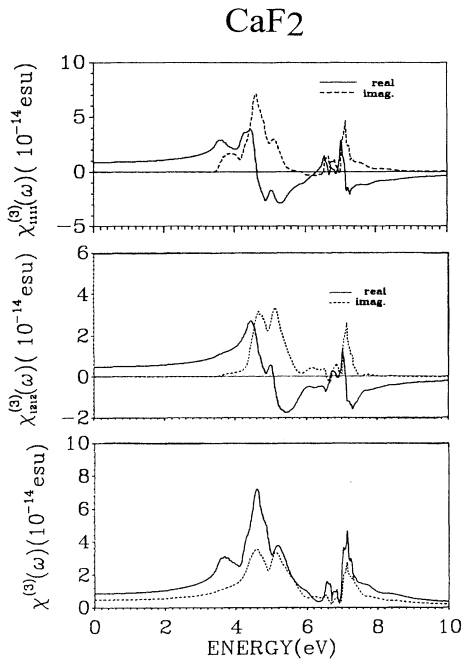


FIG. 14. Calculated THG for $CaF_2$. Notations are the same as in Fig. 10.

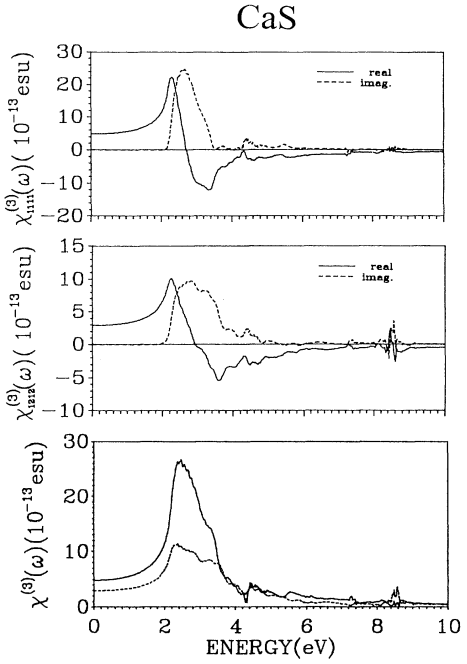


FIG. 16. Calculated THG for CaS. Notations are the same as in Fig. 10.

crystal-field and charge-transfer effects are fully reflected in the self-consistent calculation. Second, the overlap of the cation and anion wave functions is accurately accounted for. Third, interactions up to all near neighbors are included, not just the nearest neighbors. Last but not least, the anisotropic effects, which are important for certain nonlinear optical responses such as in the intensity of Raman scattering, are taken into account in a natural way.

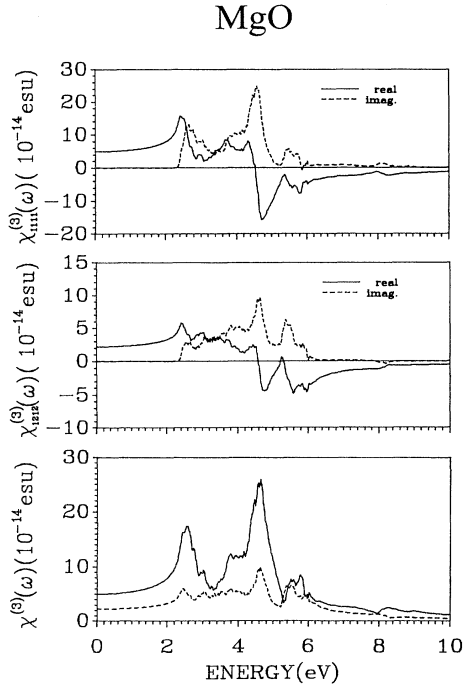


FIG. 15. Calculated THG for MgO. Notations are the same as in Fig. 10.

In reviewing the calculated data in Table II, we notice that $\chi^{(3)}(0)$ within each group can vary over two orders of magnitude as the size of the anion changes; whereas for a fixed anion, the $\chi^{(3)}(0)$ values for crystals of different cations are of the same order of magnitude. This is in agreement with the hyperpolarizability calculation of Johnson, Subbaswamy, and Senatore[26] for alkali halides, and is mainly because the anion has most of the valence electronic charge in an ionic crystal. However, for a fixed anion, the calculated $\chi^{(3)}(0)$ values do not scale with the size of the cation. This is because the present full band-structure approach involves excited CB states, which can vary considerably even for isoelectronic crystals with different cations.

To assess the validity of the calculated results, in Fig. 17 we plot the calculated values of $|\chi^{(3)}_{1111}(0)|$ and $|\chi^{(3)}_{1212}(0)|$ against the measured ones for some of the crystals. The data are taken from the measurement of Adair, Chase, and Payne[12] using nearly degenerate three-wave mixing techniques for the relative values of $n_2$. Since calibrations are needed, the data obtained in this way may have some uncertainty compared to absolute measurements. However, these data are much more reliable than those for cubic semiconductors, where large variations in the measured data for the same crystal make comparison with theory more difficult.[2,3] As can be seen from Fig. 17, the agreement between theory and experiment for $|\chi^{(3)}_{1111}(0)|$ and $|\chi^{(3)}_{1212}(0)|$ for the 14 crystals over a wide range of magnitude is quite satisfactory. For the alkali-earth fluorides, the measured data show that $CdF_2$ has $\chi^{(3)}(0)$ an order of magnitude greater than the rest in

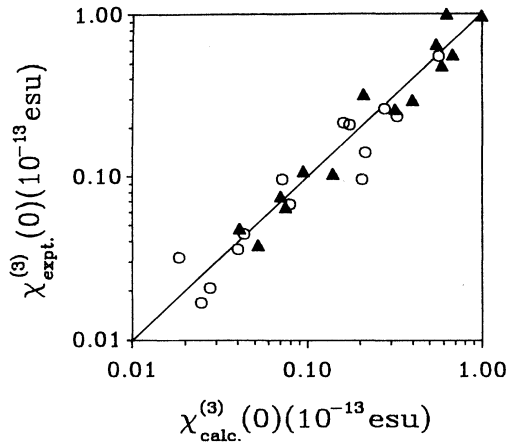


FIG. 17. Calculated $|\chi^{(3)}_{1111}(0)|(\Delta)$ and $|\chi^{(3)}_{1111}(0)|(0)$ vs the measured data from Ref. 12 for the 13 crystals: LiF, NaF, NaCl, NaBr, KF, KCl, KBr, $CaF_2$, $SrF_2$, $CdF_2$, $BaF_2$, MgO, and CaO. (See Table II.)

the series. This unique feature is faithfully reproduced by our calculation. In general, the calculated values appear to be larger than the measured ones. The differences are of the same order of magnitude as the differences between different measurements. If the gaps were not corrected, the $\chi^{(3)}(0)$ values will be slightly larger, moving away from the good agreement with data. Thus we believe that the gap correction is very important for nonlinear optical calculations using the full band-structure approach. One may recall that the improvement of the linear optical constant using the scissor operator is not a clear-cut case. However, the $\chi^{(3)}(0)$ values for the crystals studied here vary over two orders of magnitude, while that of $\varepsilon(0)$ values vary by only a factor of 2. Hence the requirement for accuracy in the linear case is far more stringent than in the nonlinear case.

In Fig. 18, we plot the calculated and experimental ratios of $|\chi^{(3)}_{1212}(0)|/|\chi^{(3)}_{1111}(0)|$ for the same 13 crystals (data for SrO was not presented). As mentioned above, this ratio is a more reliable indicator to test the band model. We also note that this ratio from different measurements for the same crystal are quite close. Of the 13 crystals, only KBr, KF, and $BaF_2$ (CaO and NaF) have somewhat underestimated (overestimated) experimental ratios. The agreement for other crystals is very satisfactory. Only KCl and $CdF_2$ have a ratio close to the isotropic value of $\frac{1}{3}$. Johnson and Subbaswamy[71] also calculated the anisotropic ratios in hyperpolarizabilities in alkali halides, and found them to be in the range of 0.3–0.37. Their calculated anisotropy is much smaller than the measured values, and may be attributed to the use of the spherical solid approximation in their calculation.

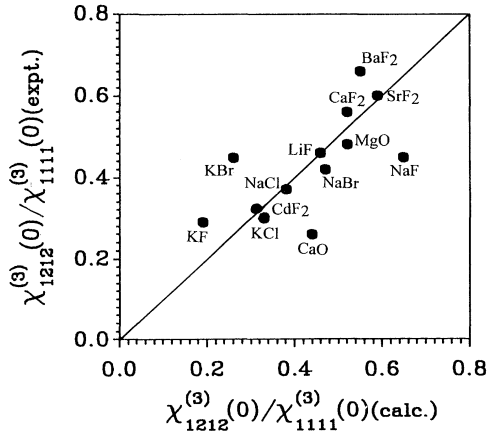


FIG. 18. Calculated ratio of $|\chi^{(3)}_{1212}(0)|/|\chi^{(3)}_{1111}(0)|$ vs experimental ones for the 13 crystals. Data converted from Ref. 12. (See Table III.)

It is also of interest to compare the present result with the other first-principles calculation of Johnson, Subbaswamy, and Senatore.[26] For alkali fluorides and chlorides, the results of the two calculations are reasonably close. However, for bromides and iodides, our calculated results are consistently larger than those of Ref. 26. We may attribute this difference to the use of pseudopotentials in the work of Ref. 26, which appears to be inadequate for crystals with heavy anions. The calculated value for $|\chi^{(3)}_{1111}(0)|$ should also be compared with that of Lines,[22,23] using the empirical bond-orbital model. (Limitation of the simple model precludes the calculation of $|\chi^{(3)}_{1212}(0)|$.) As can be seen, for most crystals, the absolute values from the bond-orbital results are much larger than the band-structure results, although the relative values appear to be much closer. Of the 11 halides for which the measured data are available, Lines renormalized both the experimental values and his calculated data for a relative comparison. He then found the root-mean-square deviation from the experimental data is only 9% for the 11 halides crystals as a group.[22] In this regard, the close agreement in the absolute values between our calculation and the data of Ref. 12 clearly demonstrates the predictive power of the present first-principles approach.

There are several directions in which the present calculations can be further improved. The inclusion of the local-field correction is probably not very important for ionic solids. This was the main conclusion of the bond-orbital calculation.[22,23] The use of a scissor operator to address the deficiency in the LDA theory appears to be adequate at the present level of precision. Inclusion of the self-energy correction and the self-interaction correction in the band-structure calculation seems to be a logical next step. However, such calculations for a large number of crystals, or for crystals with complicated structures, may be computationally too demanding. Another important aspect of improvement is the accuracy of the high CB wave functions within the LDA scheme. This can be partially accomplished by further increasing the basis size or by using different types of orbitals for basis expansion. Again, this approach will also increase computational demand tremendously. Given the fact that reliable experimental data on these crystals are still rather scarce, theoretical calculations at the present level of accuracy can provide much impetus for progress

in this area. The most promising nonlinear optical materials suitable for various optoelectronic applications are either organic polymers or inorganic crystals with structures much more complicated than cubic insulators.[72,73] Covalent or partially covalent chemical bonding may be involved. The present full band-structure approach based on the LDA-OLCAO method is fully capable of studying the nonlinear optical properties of such complex systems with no conceivable difficulties other than the computational power. The ability to calculate the dispersion relations at finite frequencies for all nonvanishing elements of the nonlinear susceptibility tensor is the strongest point of the present method, which is clearly beyond simple empirical models.

## ACKNOWLEDGMENT

This work is supported by the U.S. Department of Energy under Grant No. DE-FG02-84ER45170.

*Present address: Department of Materials Science and Engineering, MIT, Cambridge, MA 02139.

[1]M.-Z. Huang and W. Y. Ching, Phys. Rev. B **47**, 9447 (1993).
[2]M.-Z. Huang and W. Y. Ching, Phys. Rev. B **47**, 9464 (1993).
[3]W. Y. Ching and M.-Z. Huang, Phys. Rev. B **47**, 9479 (1993).
[4]Z. H. Levine and D. C. Allan, Phys. Rev. Lett. **66**, 41 (1991).
[5]Z. H. Levine and D. C. Allan, Phys. Rev. B **44**, 12 718 (1991).
[6]Hong-Ru Ma, S. T. Chui, R. V. Kasowski, and W. Y. Hsu, Opt. Commun. **85**, 437 (1991); S. T. Chui, H. Ma, R. V. Kasowski, and W. Y. Hsu, Phys. Rev. B **47**, 6293 (1993).
[7]M-Z. Huang and W. Y. Ching, Phys. Rev. B **45**, 8738 (1992).
[8]Z. H. Levine and D. C. Allan, Phys. Rev. B **48**, 7783 (1993).
[9]H. Zhong, Z. H. Levine, D. C. Allan, and J. W. Wilkins, Phys. Rev. B **48**, 1384 (1993).
[10]M.-Z. Huang and W. Y. Ching, Ferroelectrics **156**, 105 (1994).
[11]W. Y. Ching, J. Am. Ceram. Soc. **71**, 3135 (1990).
[12]R. Adair, L. L. Chase, and S. A. Payne, Phys. Rev. B **39**, 3337 (1989).
[13]H. Nanto, K. Murayama, T. Usuda, F. Endo, Y. Hirai, S. Taniguchi, and N. Takeuchi, J. Appl. Phys. **74**, 1445 (1993).
[14]S. Albin, J. D. Satira, D. L. Livinston, and T. A. Shull, Jpn. J. Appl. Phys. **31**, 715 (1992).
[15]N. L. Boling, A. J. Glass, and A. Owyoung, IEEE J. Quantum Electron. **QE-14**, 601 (1978).
[16]C. C. Wang, Phys. Rev. B **2**, 2045 (1970).
[17]M. J. Weber, D. Milam, and W. L. Smith, Opt. Eng. **17**, 463 (1978).
[18]R. Gang, Appl. Opt. **19**, 1219 (1980).
[19]J. N. Wilson and R. M. Curtis, J. Phys. Chem. **74**, 187 (1970).
[20]H. Coker, J. Phys. Chem. **80**, 2078 (1976).
[21]M. E. Lines, Phys. Rev. B **41**, 3372 (1990).
[22]M. E. Lines, Phys. Rev. B **41**, 3383 (1990).
[23]M. E. Lines, Phys. Rev. B **43**, 11 978 (1991).
[24]P. W. Fowler and P. A. Madden, Phys. Rev. B **30**, 6131 (1984).
[25]K. R. Subbaswamy and G. D. Mahan, J. Chem. Phys. **84**, 3317 (1986).
[26]M. D. Johnson, K. R. Subbaswamy, and G. Senatore, Phys. Rev. B **36**, 9202 (1987).
[27]Y.-N. Xu and W. Y. Ching, Phys. Rev. B **48**, 4335 (1993).
[28]P. Hohenberg and W. Kohn, Phys. Rev. **136**, B864 (1964); W. Kohn and L. J. Sham, *ibid.* **140**, A1133 (1965); L. J. Sham and W. Kohn, *ibid.* **145**, 561 (1965).
[29]W. E. Pickett, Comments Solid State Phys. **12**, 57 (1986).
[30]J. P. Perdew and M. Levy, Phys. Rev. Lett. **51**, 1884 (1983).
[31]L. J. Sham and M. Schlûter, Phys. Rev. Lett. **51**, 1888 (1983); Phys. Rev. B **32**, 3883 (1985).
[32]R. W. Godby, M. Schluter, and L. J. Sham, Phys. Rev. Lett. **56**, 2415 (1986); Phys. Rev. B **36**, 6497 (1987); **37**, 10 159 (1988).
[33]C. S. Wang and W. E. Pickett, Phys. Rev. Lett. **51**, 597 (1983); Phys. Rev. B **30**, 4719 (1984).
[34]M. S. Hybertsen and S. G. Louie, Phys. Rev. Lett. **55**, 1418 (1985); Phys. Rev. B **34**, 5390 (1986); **37**, 2733 (1988).
[35]P. A. Sterne and J. C. Inkson, J. Phys. C **17**, 1497 (1984); S. J. Jenkins, G. P. Srivastava, and J. C. Inkson, Phys. Rev. B **48**, 4388 (1993).
[36]W. Hanke and L. J. Sham, Phys. Rev. B **38**, 13 361 (1988).
[37]F. Bechstedt and R. Del Sole, Phys. Rev. B **38**, 7710 (1988).
[38]S. B. Zhang, D. Tománek, M. L. Cohen, S. G. Louie, and M. S. Hybersten, Phys. Rev. B **40**, 3162 (1989).
[39]F. Gygi and A. Balderechi, Phys. Rev. Lett. **62**, 2160 (1989).
[40]X. Zhu and S. G. Louie, Phys. Rev. B **43**, 14 142 (1991).
[41]M. Rohlfing, P. Krüger, and J. Pollman, Phys. Rev. B **48**, 17 791 (1993).
[42]L. Fritsche and Y. M. Yu, Phys. Rev. B **48**, 4250 (1993).
[43]Z. Q. Gu and W. Y. Ching, Phys. Rev. B **49**, 10 958 (1994).
[44]D. J. Moss, E. Ghahramani, J. E. Sipe, and H. M. van Driel, Phys. Rev. B **41**, 1542 (1990).
[45]E. Ghahramani, D. J. Moss, and J. E. Sipe, Phys. Rev. B **43**, 9700 (1991).
[46]F. Perrot, Phys. Status Solidi **52**, 163 (1972).
[47]N. E. Brener, Phys. Rev. B **11**, 1600 (1975).
[48]A. Zunger and A. J. Freeman, Phys. Rev. B **16**, 2901 (1977).
[49]J. P. Albert, C. Jouanin, and G. Goat, Phys. Rev. B **16**, 4619 (1977).
[50]R. A. Heaton and Chun C. Lin, Phys. Rev. B **22**, 3629 (1980).
[51]A. B. Kunz, Phys. Rev. B **26**, 2056 (1982).
[52]N. C. Amaral, B. Maffeo, and D. Guenzburger, Phys. Status Solidi B **117**, 141 (1983).
[53]J. Yamashita and S. Asano, J. Phys. Soc. Jpn. **52**, 3506 (1983); **53**, 3112 (1984).
[54]M. Causà, R. Dovesi, C. Pisani, and C. Roetti, Phys. Rev. B **33**, 1308 (1986).
[55]M. J. Mehl, R. E. Cohen, and H. Krakauer, J. Geophys. Res. **93**, 8009 (1988).
[56]V. S. Stepanyuk, A. Szasz, O. V. Farberovich, A. A. Grigorenko, A. V. Kozlov, and V. V. Mikailin, Phys. Status Solidi B **155**, 215 (1989).
[57]R. Pandey, J. E. Jaffe, and A. B. Kunz, Phys. Rev. B **43**, 9228 (1991).
[58]Y.-N. Xu and W. Y. Ching, Phys. Rev. B **43**, 4461 (1991).
[59]F. Gan, M. Z. Huang, Y.-N. Xu, W. Y. Ching, and J. G. Harrison, Phys. Rev. B **45**, 8248 (1992).
[60]K. C. Mishra, K. H. Johnson, and P. C. Schmidt, Mater. Sci. Eng. B **18**, 214 (1993).
[61]O. Schütt, P. Pavone, W. Windl, K. Karch, and D. Strauch, Phys. Rev. B **50**, 3746 (1994).
[62]N. C. Pyper, Adv. Solid State Chem. **2**, 223 (1991).

[63]Y.-N. Xu and W. Y. Ching, Phys. Rev. B **44**, 7787 (1991); **44**, 11 048 (1991).
[64]W. Y. Ching and Y.-N. Xu, Phys. Rev. B **44**, 5332 (1991).
[65]S. Loughlin, R. H. French, W. Y. Ching, Y.-N. Xu, and G. A. Slack, Appl. Phys. Lett. **63**, 1182 (1993).
[66]Y.-N. Xu and W. Y. Ching, Phys. Rev. B **48**, 17 695 (1993).
[67]R. H. French, S. J. Glass, F. S. Oguchi, Y.-N. Xu, and W. Y. Ching, Phys. Rev. B **49**, 5133 (1993).
[68]W. Y. Ching, L. Liu, and Y.-N. Xu, Ferroelectrics **153**, 25 (1994).
[69]D. Maker and R. W. Terhune, Phys. Rev. **137**, A801 (1965).
[70]M. D. Levenson and N. Bloembergen, Phys. Lett. **50A**, 61 (1974).
[71]M. D. Johnson and K. R. Subbuswarmy, Phys. Rev. B **39**, 10 275 (1989).
[72]A. M. Glass, Science **226**, 657 (1984).
[73]D. F. Eaton, Science **253**, 281 (1991).